Formation and Characterization of Pt Nanoparticle Networks

Fei Wen,[a] Norbert Waldöfner,[a] Wolfgang Schmidt,[a] Klaus Angermund,[a] Helmut Bönnemann,*[a] Stephanie Modrow,[b] Svetlana Zinoveva,[b] Hartwig Modrow,[b] Josef Hormes,[c] Lars Beuermann,[d] Sergiy Rudenkiy,[d] Wolfgang Maus-Friedrichs,[d] Volker Kempter,[d] Thomas Vad,[e] and Heinz-Günter Haubold[e]

Keywords: Colloids / Cross-linking / Nanostructures / Platinum / Self-assembly

Nanoparticle networks can be synthesized by the self-assembly of arrays of metal colloid particles linked by spacer molecules of different sizes. The particles are linked through reactive aluminum sites in a metal–organic shell around the metal particles. Rigid spacer molecules with functional groups at each end are used to bind at these reactive sites. The resulting networks have been characterized by various methods such as transmission electron microscopy (TEM), sorption analysis, X-ray absorption spectroscopy (XAFS), anomalous small angle X-ray scattering (ASAXS), metastable impact electron spectroscopy (MIES), and ultraviolet photoelectron spectroscopy (UPS). These investigations showed that the metal nanoparticles form aggregated networks with average distances between the metal particles that are determined by the sizes of the spacer molecules applied. In this way, porous as well as nonporous networks have been obtained. Whether accessible pores are formed depends on the type of spacer molecule. Furthermore, the properties of the metal particles have proved to be sensitive towards the reaction of the aluminum in the protective shells with the linker molecules.

(© Wiley-VCH Verlag GmbH & Co. KGaA, 69451 Weinheim, Germany, 2005)

Introduction

The assembly of nanosized metal particles into highly ordered arrays has become a new trend in chemistry over the past few years.[1–3] The resulting materials are expected to exhibit novel collective properties that make them very promising with respect to application in microelectronics or optics.[4,5] Superlattices of nanocrystals have already been reported,[6–12] but bottom-up syntheses of three-dimensional structures consisting of nanoparticles still remain a challenge for the synthetic chemist. Over the past couple of years we have developed a synthetic strategy for the preparation of arrays of three-dimensionally connected nanoparticles. The key feature of this synthesis is the formation of a reactive metal–organic colloidal protecting shell around the particles.[13] Reactive alkylaluminum groups in the protective shell allow substitution of the alkyl groups by other organic groups,[14] and the use of bifunctional substituents allows the linking of two metal particles and, consequently, the formation of larger networks of metal particles.[15,16] Using this approach it possible to cross-link different types of metal nanoparticles, such as Pt, Ni, and Co. The synthetic procedures have been adapted to the specific chemistry of the metal species, and the suitability of different alkyl groups in the protective shell has been investigated. The present review gives a survey of these results. In order to provide a consistent thread, however, we will focus here mainly on cross-linked Pt nanoparticles.

[a] Max-Planck-Institut für Kohlenforschung, Kaiser-Wilhelm-Platz 1, 45470 Mülheim an der Ruhr, Germany
[b] Physikalisches Institut der Universität Bonn, Nussallee 12, 53115 Bonn, Germany
[c] Center for Advanced Microstructures and Devices, 6980 Jefferson Hwy, Baton Rouge, LA 70806, USA
[d] Institut für Physik und Physikalische Technologien, Technische Universität Clausthal Leibnizstraße 4, 38678 Clausthal-Zellerfeld
[e] Forschungszentrum Jülich, Institut für Festkörperforschung, 52425 Jülich

Synthesis of Pt Colloids

Different colloid particles, i.e. Pt, Ni, and Co, are considered in this survey, although the general synthetic concept will be demonstrated for Pt particles. In a typical synthesis, the Pt colloids were prepared as follows: $Pt(acac)_2$ (1.97 g, 5 mmol) was dissolved in 200 mL of toluene. Then, $Al(CH_3)_3$ (1.44 g, 20 mmol) was dissolved in 200 mL of tol-

MICROREVIEWS: This feature introduces the readers to the authors' research through a concise overview of the selected topic. Reference to important work from others in the field is included.

uene and carefully added to the first solution over 4 h at 60 °C. After the gas evolution had stopped (24 h), the solution was filtered, and all volatile components were completely evaporated under vacuum to give 2.4 g of colloidal platinum powder in the form of a black, air-sensitive powder. The Pt colloid used for the experiments described here had a composition of 40% Pt, 14% Al, 31% C, and 6% H (by elemental analysis).

H. Bönnemann studied chemistry at the RWTH Aachen, Germany, where he received his PhD and habilitation. After two years of industrial research at Degussa, he became Professor for Industrial Chemistry at the RWTH Aachen, Germany, in 1981. Later on, he worked at the Max-Planck-Institut für Kohlenforschung in Mülheim an der Ruhr, Germany, where he installed a research group with focus on nanoparticles and colloidal metals. In 2004 he became a scientific member of the Forschungszentrum Karlsruhe, Germany, where he has worked as leader of the Nanochemistry Laboratory at the Institute for Industrial Chemistry since January 2005. Fei Wen and Norbert Waldöfner worked as PhD students in his laboratory at the Max-Planck-Institut für Kohlenforschung.

Wolfgang Schmidt studied Chemistry at the University of Mainz, Germany, where he received his PhD in 1994. During his PhD studies, he had a research term at the Boreskov Institute of Catalysis in Novosibirsk, Russia. From 1995 to 1998, he worked as staff scientist at the University of Frankfurt and then became senior scientist in the Department of Heterogeneous Catalysis at the Max-Planck-Institut für Kohlenforschung in Mülheim an der Ruhr. His work is focused on the preparation and characterization of nanoparticles and porous materials.

Klaus Angermund studied chemistry at the Heinrich-Heine University of Düsseldorf, Germany. From 1983 to 1986, he worked as a PhD student in the X-ray department at the Max-Planck-Institut für Kohlenforschung in Mülheim an der Ruhr, Germany. In 1986, he obtained his Ph D in Chemistry from the University of Wuppertal, Germany. In 1987, he was awarded the Otto Hahn scholarship by the Max-Planck Society and worked from 1987 to 1988 as a postdoctoral fellow with Arnold Hagler at Biosym Technologies Inc. in San Diego (USA). Since 1989 he is a scientific co-worker at the Max-Planck-Institut für Kohlenforschung and head of the molecular modeling group. His research focuses on application of molecular modeling techniques to organometallic reactions, force field development and parameterization, and QM/MM methods.

Hartwig Modrow received his PhD in Physics from the University of Bonn, Germany, in 1999. At present, he is Oberassistent at this institute and acting head of the synchrotron radiation group, which specializes in the investigation of electronic and geometric structure of matter and their dynamics. Stephanie Modrow obtained her PhD in that group and is presently working as a patent attorney. Svetlana Zinoveva has been pursuing her PhD Thesis work in the synchrotron radiation group since 2003.

Josef Hormes studied Physics at the University of Bonn, Germany, where he received his PhD in 1975 and habilitation in 1984. After working for the University of Bonn, the Imperial College of London, and Stockholm University (Sweden), he was appointed Professor for Physics at the University of Bonn in 1988. In the period from 1988 to 1999, he was also the Director of the Synchrotron Radiation Laboratory at the University of Bonn. Since 1999, he is Director of the Center for Advanced Microstructures & Devices at the Louisiana State University (LSU) in Baton Rouge, USA, and Professor in the Department of Physics and Astronomy at LSU.

Volker Kempter received his Ph.D. in Physics from the University of Freiburg, Germany, in 1969. He is Prof. of Physics at the Technical University of Clausthal, Germany, where he leads the section for "Molecular Processes on Surfaces". His group specializes on the oxidation and corrosion of films and nanoparticles and on processes on ice surfaces. Lars Beuermann and Sergiy Rudenkiy work as PhD students in his group and Dr. Wolfgang Maus-Friedrichs, as senior scientist, focuses on the investigation of surfaces with relevance for applications in material science.

Heinz-Günter Haubold was leader of the SAXS group at the Institut für Festkörperforschung at the Forschungszentrum Jülich from where he retired in 2003. He designed and built up the user-dedicated ASAXS experiment JUSIFA at the synchrotron facility of HASYLAB at DESY Hamburg, Germany. His coworker Thomas Vad worked on the development of routines and models for the interpretation of ASAXS data.

 © 2005 Wiley-VCH Verlag GmbH & Co. KGaA, Weinheim

Formation of Pt Colloid Networks

As described above, Pt colloid particles were prepared by reducing $[Pt(acac)_2]$ with $Al(CH_3)_3$. These particles have highly reactive methylaluminum groups in the colloidal stabilizer, which allows protonolytic reactions at the protective shell with alcohols or carboxylic acids, while the metallic core remains intact. Several bifunctional organic spacer molecules have been used to cross-link the Pt colloid to form nanoparticle networks. One example using hydroquinone as the spacer is illustrated in Scheme 1.

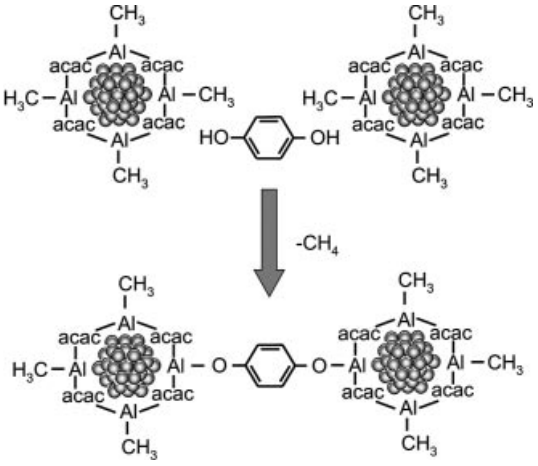

Scheme 1. Principle of the protonolytic cross-linking mechanism.

Further spacer molecules used to cross-link protected colloid particles are shown in Scheme 2. The spacer compounds HBDB, HBP, and HPDB were kindly supplied by Prof. Dr. Joannis Kallitsis[17,18] of the Institute of Chemical Engineering at the University Patras, Greece. For simplicity, the abbreviations given in the scheme will be used when discussing the different molecules.

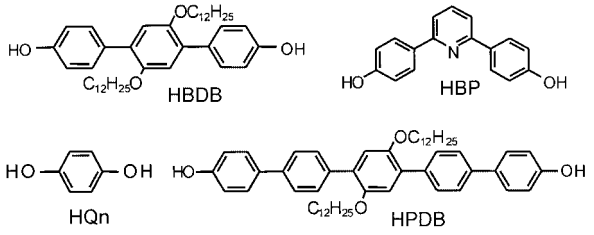

Scheme 2. Structures of the molecular spacers.

All reactions were performed in THF. The ratio of methylaluminum groups in the colloid to hydroxy groups in the molecular spacer was found to be 1:1. The molecular spacers were added dropwise into the Pt colloidal solution over 1 h. The quantity of reactive methylaluminum groups in the colloidal shell can be measured on the basis of the amount of gas (methane) evolved upon adding acetic acid to the Pt colloid. Since the reactive methylaluminum groups are statistically present on the colloidal surfaces, a 3D cross-linked nanoparticle network can be expected. The precipitate formed after the cross-linking reaction between the Pt colloid and the bifunctional molecular spacers can be isolated by simple filtration.

In the present work, several molecular spacers with different rigidity have been used to prepare Pt nanoparticle networks; their structures are depicted in Scheme 2. Here we will focus mainly on the more-rigid molecules hydroquinone (HQn), HBP, HBDB, and HPDB rod-like structures. The spacer lengths depend more or less on their conformational structures.

The introduction of HBDB and HPDB into the Pt colloidal solution caused a precipitate to form in 2 h. Compared with the results using hydroquinone and HBP as the spacers, these precipitates were produced rapidly and were very loosely suspended in the reaction medium. For some samples, the preparation conditions were varied to investigate the effect of this variation on the properties of the resulting materials. For example, the sample Pt/HBP was synthesized at 50 °C, while another sample, Pt/HBP2, was prepared at 25 °C using the same spacer molecule. In a similar manner, Pt/HBDB and Pt/HBDB2 were prepared at 50 and 25 °C, and Pt/HPDB and Pt/HPDB2 at 25 and 50 °C, respectively.

Characterization Methods

Transmission Electron Microscopy (TEM)

TEM measurements were performed using a Hitachi H 7500 instrument operating at an accelerating voltage of 120 kV. Energy-dispersive X-ray spectroscopy (EDX) analyses were performed to obtain a chemical analysis of the particles using an Oxford Instruments INCA EDX spectrometer attached to the microscope. The TEM samples were prepared by placing a drop of the colloidal dispersion onto a copper grid coated with a carbon film. High-resolution TEM measurements were performed on a Hitachi HF 2000 Instrument operating at 200 kV. In order to obtain a chemical analysis of the bimetallic catalysts, point-resolved EDX analyses were performed using a Noran Instruments EDX spectrometer attached to the microscope. The samples were prepared by placing a drop of the colloidal dispersion onto a copper grid coated with a lacey film.

Physisorption Analysis

Nitrogen sorption isotherms were recorded with a Micromeritics ASAP 2010 sorption analyzer at 77 K to evaluate the textural properties of the prepared porous materials. Prior to the measurements, the samples were evacuated at 80 °C for 12 h. The BET (Brunauer–Emmett–Teller) surface area was calculated from the adsorption data in the relative pressure interval from 0.06 to 0.20.

Anomalous Small-Angle X-ray Scattering (ASAXS)

For the characterization of nanostructures with typical metal-particle diameters and interparticle distances in the 1–10 nm regime, small-angle X-ray scattering (SAXS) is amenable for the determination of the structure parameters. Thus, anomalous small-angle X-ray scattering (ASAXS)

 © 2005 Wiley-VCH Verlag GmbH & Co. KGaA, Weinheim

was applied to analyze the inter-particle distances of the as-prepared Pt network products, as the contributions from the organic parts and pore-like voids can be subtracted. Different Pt samples[15] were investigated by ASAXS at the JUSIFA beamline[19] at HASYLAB (DESY Hamburg, Germany). The contrast variation experiments were performed at two X-ray energies, namely E_1 = 11.437 keV and E_2 = 11.535 keV, near the Pt L_3 [$E(L_3)$ = 11.564 keV] absorption edge (for a detailed description, see ref.[16]).

Since ASAXS is not a very common characterization method, the principle of ASAXS measurements will be introduced here.

In the case of a low-concentration ensemble of uniform metal particles in a (negligible) low-molecular matrix, the particle scattering intensity can be written as:

$$\frac{d\Sigma}{d\Omega}(Q) = c_0 n^2 f_0^2 S^2(Q) V^2,$$

where c_0 (= $Nanoparticle_{\text{article}}/V_{\text{sample}}$) is the number density of the particles, n [= N_{atoms}/V (V = particle volume)] is the number density of the metal atoms within a particle, f_0 is the scattering amplitude, and $S^2(Q)$ is the intraparticle interference factor, i.e., the form factor of a particle.

For a spherical particle of radius R_0, the particle form-factor is defined by

$$S(Q) = 3\frac{\sin(QR_0) - QR_0\cos(QR_0)}{(QR_0)^3},$$

with the magnitude of the scattering vector Q being equal to $4\pi\sin\Theta/\lambda$ (λ is the X-ray wavelength and 2Θ is the scattering angle). In order to obtain more information on the (pure) particle scattering, it is convenient to perform ASAXS experiments. For the two-phase model, the total differential cross-section is given by

$$\frac{d\Sigma}{d\Omega}(Q) = c_0(n_p f_p - n_m f_m)^2 S^2(Q) V^2 + \frac{d\Sigma}{d\Omega_{bg}}(Q),$$

where n_p, f_p, n_m, and f_m are the number densities and atomic form-factors, respectively, of the particles (p) and the surrounding matrix (m). Besides the particle scattering, an additional background scattering term $d\Sigma/d\Omega_{bg}(Q)$ (which is proportional to Q^{-4} in most cases) contributes to the total differential cross-section, which, for the most part, originates from inhomogeneities in the matrix. Therefore, the SAXS intensity almost always contains a (in many cases non-negligible) contribution from the matrix if a SAXS experiment is performed at only one energy. Fortunately, the particle scattering can quite easily be separated from the matrix background if, for example for Pt particles, contrast-variation experiments are carried out at at least two different energies near the Pt L_3 absorption edge [E(Pt L_3) = 11564 eV]. As shown schematically in Figure 1, the atomic form-factors of the Pt particles vary significantly at energies close to the absorption edge, while those of all other elements, i.e. the matrix, remain more or less constant.

Thus, the atomic form-factors

$$f(E) = f_0 + f'(E) + if''(E)$$

of the mainly organic matrix components (C, H, O) remain almost constant in this energy regime. A simple subtraction of two SAXS curves measured at two different energies E_1 and E_2 yields the (almost) pure (Pt) metal-particle scattering

$$\frac{d\Sigma}{d\Omega_p}(Q) = \frac{d\Sigma}{d\Omega}(Q,E_1) - \frac{d\Sigma}{d\Omega}(Q,E_2)$$
$$= c_0 n^2\left[f_{Pt}^2(E_1) - f_{Pt}^2(E_2)\right]S^2(Q)V^2 \times \left\{1 - \frac{2n_m f_m}{n\left[f_{Pt}(E_1) + f_{Pt}(E_2)\right]}\right\}$$

(in the case of negligible f'' correction terms), which reduces to

$$\frac{d\Sigma}{d\Omega_p}(Q) = c_0 n^2\left[f_{Pt}^2(E_1) - f_{Pt}^2(E_2)\right]S^2(Q)V^2$$
$$= c_0\Delta(nf)^2 S^2(Q)V^2$$

$$\text{if } 2n_m f_m / \{n\left[f_{Pt}(E_1) + f_{Pt}(E_2)\right]\} \ll 1.$$

From the scattering curves thus obtained, the average particle sizes and particle–particle distances are accessible. Figure 2 shows how the thickness of the protective layer and the average distance between particles that are linked by different spacer molecules are accessible from the

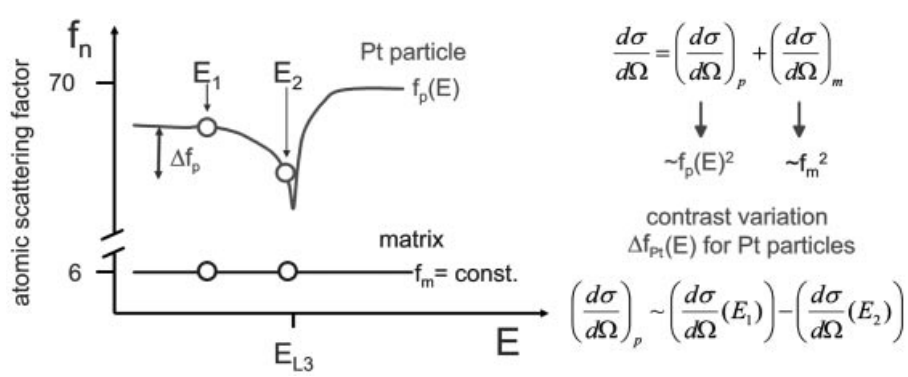

Figure 1. Schematic representation of the dependence of atomic scattering factors from the energies close to the absorption edge of an element (here Pt).

ASAXS data. Knowing the size (R_0) of the pure colloid particle allows calculation of the thickness of the protective shell (t_{ps}) from the particle–particle distance if the protected particles have direct contact, i.e. in solid aggregates of protected particles without spacer molecules. The distance (D_0) between cross-linked particles then allows calculation of the distance (l_{sp}) due to the spacer molecules by considering the thickness of the protective layer according to $l_{sp} = D_0 - (2t_{ps})$.

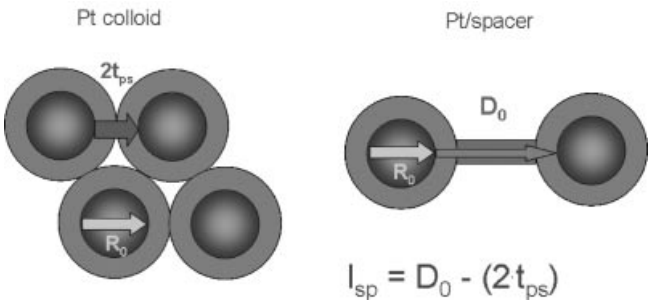

Figure 2. Model to calculate the thickness of the protective layer, t_{ps}, and the distance due to the spacer molecule, I_{sp}, from the particle–particle distance, D_0 (R_0 is the radius of the colloid particle, here Pt colloid).

X-ray Absorption Spectroscopy (XAFS)

The X-ray absorption spectra discussed in this article were measured in transmission mode at two different synchrotron radiation sources: at the ELSA storage ring at University of Bonn, Germany, and at the Center for Advanced Microstructures and Devices (CAMD). Detailed descriptions of the beamlines and instrumentation are found in the literature;[20,21] important parameters of the measurements are summarized in Table 1.

To prepare the samples for measurement at the Al K-edge, a very thin but homogeneous and pinhole-free layer of powder was fixed on an ultra-thin (6 μm) polypropylene film by application of pressure. For all other measurements, the dried colloids were mixed with boron nitride and pressed into pellets. The optimal sample thickness was found by trial and error and was chosen in such a way that the maximum absorption, μd, was not higher than 1.2. The entire process of sample preparation was undertaken in a glove box filled with argon. Sample transfer to the measurement station also took place under an inert gas atmosphere.

XANES data treatment consisted of subtraction of a linear background adapted to the pre-edge and normalization to an edge jump of one at the position given in Table 1. For EXAFS analysis, the UWXAFS package[22] was used.

Metastable Impact Electron Spectroscopy (MIES) and Photoelectron Spectroscopy (UPS)

The characterization of the surface of metal nanoparticles (nanoparticle) is of considerable technological relevance as:

- often a pre-stabilization, i.e. passivation of the particles against air and/or moisture, is required when it is planned to integrate them into nanostructures (or particle networks as in the present application);
- a termination of the nanoparticles by some particular active molecular group, with bifunctional character in the present case, is required in order to be able to interlink the nanoparticles within a customized nanostructure or particle network;
- some applications require a peptization of the nanoparticles, i.e. their embedding into a micelle of specific organic molecules, in order to prevent sintering of the reactive nanoparticles.

Thus, the availability of techniques that are able to concentrate specifically on the chemical properties and the electronic structure of the outermost layer of the nanoparticles is mandatory in order to design, characterize, and manipulate nanoparticles in particle networks or nanostructures in general. Ideally, the depth resolution of the employed surface-analytical technique should be tunable in the sense that, besides the information on the outermost layer, the corresponding information on the sub-surface region of the particles should also be provided for comparison.

MIES metastable He atoms are utilized to eject electrons from surfaces. Metastable He* atoms with thermal energy interact with condensed matter, including nanoparticles, by three different mechanisms depending on the electronic structure of the surface under consideration and its work function.[23,24] In the present work, only Auger neutralization (AN) and Auger deexcitation (AD) are observed. When molecular adsorption onto metals is studied, the situation can become complicated as a change of the mechanism from AN (on clean metals) to AD often takes place as a function of the adsorbate coverage because either an insulating surface is formed or the transfer of the He 2s electron into the metal, which is a prerequisite for the AN process, becomes inhibited because the metal becomes increasingly shielded by adsorbed species from access by the He* probe atoms.

Table 1. Results of Pt L_{III} EXAFS analysis for unconnected and two differently connected nanoparticle systems. Fitting was done in r-space between 0.15 and 0.32 nm using a k-weight of 3.

Pt L_3 Edge	Backscatterer	R [nm]	N	σ^2 [nm^2]	E_0 [eV]
Unconnected	Al	0.248 ± 0.002	0.8 ± 0.4	$2\times10^{-5}\pm3\times10^{-5}$	0.1 ± 6.3
	Pt	0.270 ± 0.002	4.0 ± 3.3	$11\times10^{-5}\pm6\times10^{-5}$	–0.5 ± 3.6
Connected	O	0.07 ± 0.001	0.7 ± 0.1	$5\times10^{-5}\pm1\times10^{-5}$	8.1 ± 1.6
(sebacic acid)	Al	0.253 ± 0.001	0.4 ± 0.1	$2\times10^{-5}\pm2\times10^{-5}$	2.9 ± 2.8
	Pt	0.267 ± 0.001	4.7 ± 0.6	$9\times10^{-5}\pm1\times10^{-5}$	0.9 ± 0.8
Connected	Al	0.250 ± 0.001	0.8 ± 0.1	$4\times10^{-5}\pm8\times10^{-5}$	11.4 ± 1.6
HBP	Pt	0.279 ± 0.001	6.2 ± 1.4	$2\times10^{-5}\pm1\times10^{-5}$	11.4 ± 1.6

 © 2005 Wiley-VCH Verlag GmbH & Co. KGaA, Weinheim

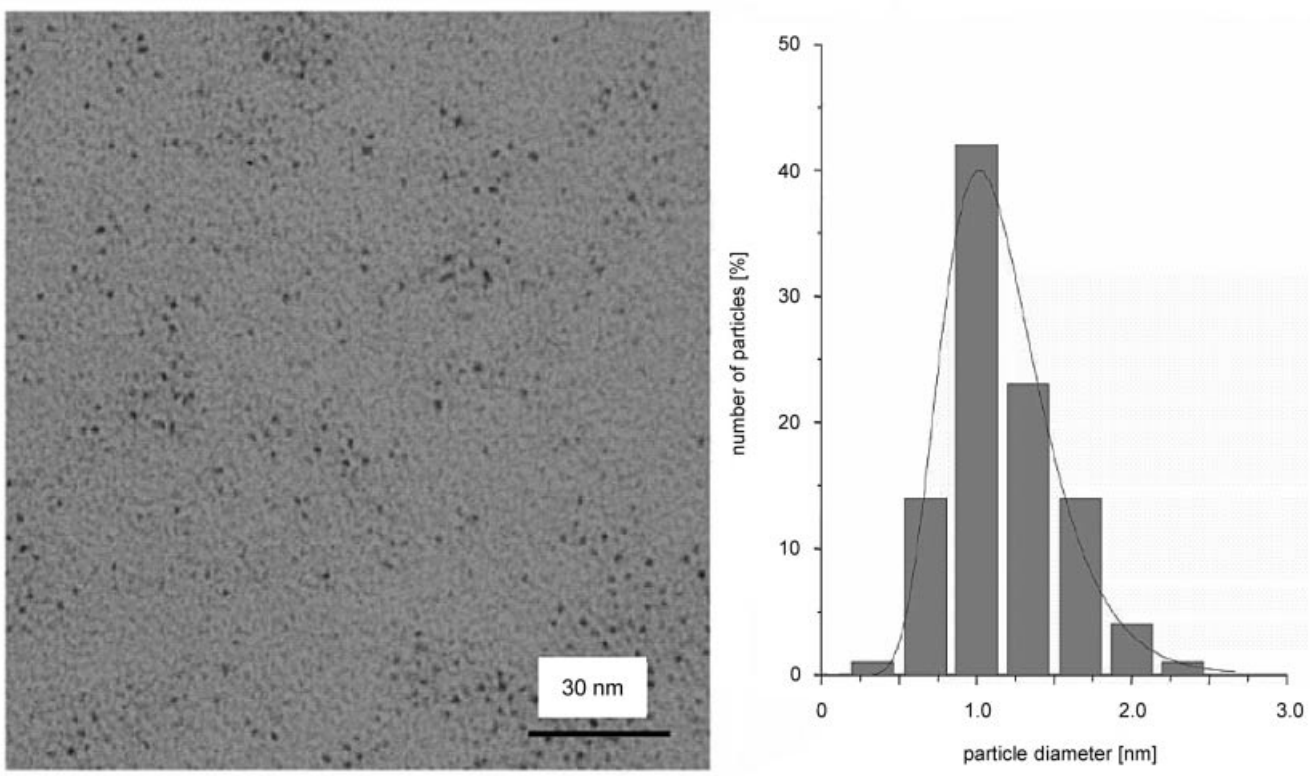

Figure 3. a) TEM image of Pt colloid particles and b) the corresponding particle size distribution (from ref. 16 with permission from IUCr).

While the energy balance of MIES (at least for the AD process) is quite similar to that of UPS (HeI) the depth information of MIES is "zero" because the Auger processes typically take place 4 a.u. in front of the surface and electrons are ejected from species in the outermost layer of the nanoparticles. On the other hand, the depth information of UPS (HeI) is about three monolayers (ML), therefore this technique provides information on the sub-surface region, although averaged over three monolayers. A more detailed introduction to MIES and its various applications in molecular and surface spectroscopy can be found in recent reviews.[23,24] Details of the apparatus employed for the present work can be found elsewhere.[25–27] For the characterization of the chemical composition of the bare surface as well as of films of nanoparticles the apparatus was equipped with a twin anode (Mg/Al) XPS source.

Characterization of Pt Colloids

TEM, ASAXS, and Sorption Analysis

A TEM image of the Pt colloid sample used and the respective particle size distribution is shown in Figure 3. The particles have an average diameter of 1.2 nm.

The particle sizes were confirmed by small-angle X-ray scattering experiments. The particle sizes determined for the Pt colloids by ASAXS were 1.2 ± 0.06 nm. The average distance between neighboring Pt particles in this solid was determined by ASAXS to be 0.36 nm. Assuming a direct contact between the protected particles, the thickness of the protective layer is thus 0.18 nm.

After evaporation of the solvent, nitrogen sorption experiments on the obtained powder resulted in specific surface areas (BET) in the range of only a few square meters per gram. From geometric considerations, spherical 1.2-nm Pt particles should have a specific surface area of about $230\ m^2\,g^{-1}$. This discrepancy can be explained by the extremely small voids that form between densely packed particles of this size − the nitrogen molecules are simply too large to fit into these voids. Thus, only the external surface areas of the Pt particle aggregates contribute to the BET surface area. The majority of the colloid particle surfaces are inside the aggregates and thus not accessible to the nitrogen.

XAFS Characterization of Particles Before Networking

Figure 4 shows the Pt L_3-edge XANES spectra of the Pt nanoparticles that, along with the spacer molecules, form the basic building blocks of the cross-linked systems under investigation in this study. Evidently, clear differences with the reference spectrum of a Pt foil are observed. For example, the characteristic resonances of the reference spectrum are present, but strongly damped. This is to be expected for nanoscaled systems. One reason for this resides in the large number of surface atoms (in this case about 75%) that do not possess complete nearest neighbor shells and for which surface relaxation effects prevent the ideal coherent addition of scattering paths. In addition, nanoscaled particles

 © 2005 Wiley-VCH Verlag GmbH & Co. KGaA, Weinheim

frequently show increased local disorder, which is not described well using the standard Debye–Waller factor approach due to its partially anharmonic nature. A detailed discussion of such effects on nanoparticles[28–30] and a thorough general discussion of the consequences of such inharmonicity[31] can be found in the literature.

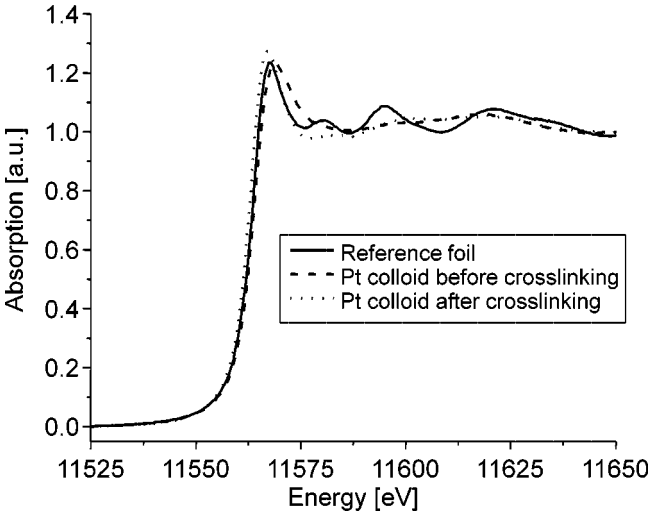

Figure 4. Pt L_3 XANES spectra of (top to bottom): Pt reference foil, Al-organically stabilized Pt colloid after cross-linking with sebacic acid, the same material before cross-linking. Measurements were performed at CAMD.

Intuitively less to be expected are the changes observed in the white-line area, where electronic rather than geometric structure is probed. The maximum intensity of the white-line feature is slightly reduced and shifted to higher excitation energy and features a less-steep slope to the high energy side. Calculations performed in the context of a previous in situ study on the synthesis of such particles[32] suggest that this can indicate an effect of a Pt–Al coordination to surface atoms.

These results are in agreement with the corresponding EXAFS analysis, whose results are summarized in Figure 5 and Table 1: in addition to the expected Pt–Pt coordination at a distance, which is slightly reduced relative to the Pt–Pt distance encountered in bulk Pt, an additional backscatterer located at a distance of about 2.5 Å is needed in order to achieve a fit with reasonably good quality. Clearly, this distance is too high for a second row element such as O or C, but is in good accordance with the distance expected for a coordinated Al atom. A more detailed discussion of the EXAFS analysis of the particles before cross-linking can be found in a previous publication.[33]

MIES and UPS

The concept of the surface characterization of nanoparticles is as follows. Normally, the metal particles need a "shell" that serves two purposes:

· *Passivation*: the long-term stability of the metal particles (the magnetic particles Fe, Ni, and Co in particular) against

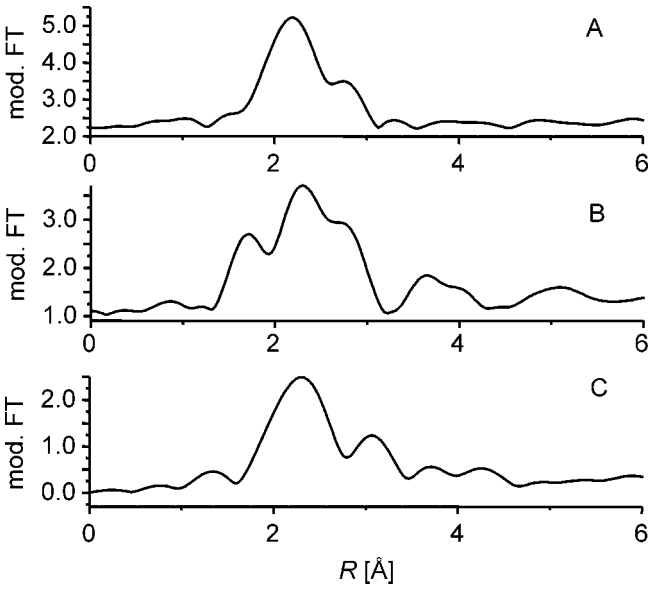

Figure 5. Non-phase-corrected radial distribution functions of (from top to bottom): a) the colloid before cross-linking, b) the colloid network with sebacic acid spacer, c) the colloid networked with HBP.

air and/or moisture has to be guaranteed prior to their integration into a nanoparticle network or, more generally, into a nanostructure;

· *Anchor Function*: the shell must allow for the reliable embedding of the nanoparticles into the custom-designed network, i.e. for the reliable interlinking of the particles in the network by "spacer" molecules.

In general, a two-step procedure must be pursued in order to get information on the composition and the electronic structure of the particles' shell:

· A planar film of the species from which the nanoparticles, Pt in the present case, are composed, has to be studied by MIES and UPS, eventually supported by techniques that give additional information on the chemical composition of the metal film prior to and after being subjected to the shell molecules (XPS), and on the film topology (STM). Then, the interaction of selected atomic and/or molecular species ("shell molecules"; see below) with this film has to be studied in the same way. This step provides "fingerprint spectra" that provide structural information that can be compared with that obtained in the second step on the nanoparticles from the same species as those that constitute the film, and also provide structural information on those molecules that potentially form the shell of the nanoparticles.

· The corresponding analysis is performed on the nanoparticles, which normally possess a shell resulting from wet-chemical procedures. An obvious complication arises from the fact that the composition of the shell produced in this way is, a priori, unknown, i.e. normally cannot be predicted on the basis of the wet-chemical procedures alone. A comparison of the results from the second step with a series of "fingerprint spectra", which have either been gathered in

 © 2005 Wiley-VCH Verlag GmbH & Co. KGaA, Weinheim

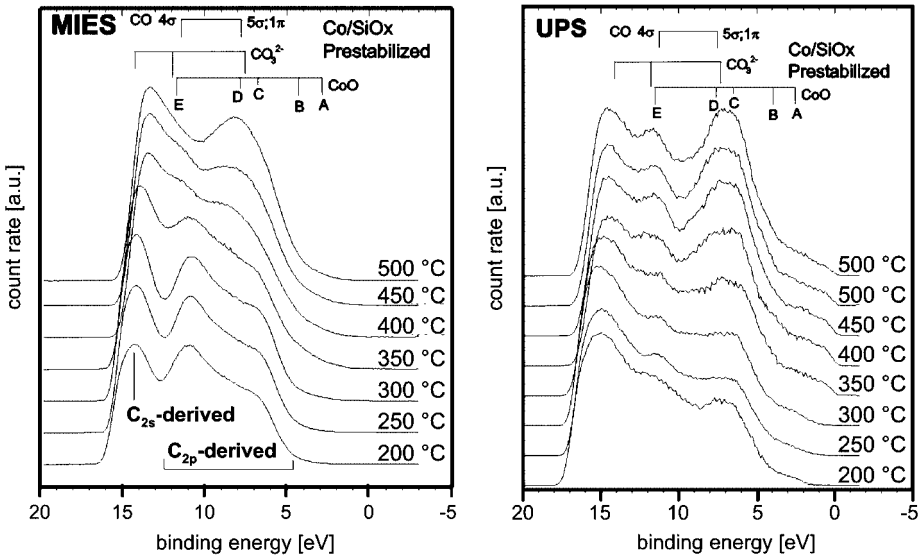

Figure 6. MIES and UPS spectra of Co nanoparticles pre-stabilized by soft oxidation. Deposition on SiO_x. The substrate temperature after deposition was varied between 200 and 500 °C.

the first step or are already available in the literature, is required.

For didactic reasons, the details of the above-mentioned procedure will be illustrated for Co nanoparticles possessing a shell produced by "soft oxidation". First, Co films were produced on SiO_x. These films were then exposed to O_2, CO, and CO_2 with in situ control by MIES/UPS. A detailed presentation of the results and their interpretation can be found elsewhere.[34] Secondly, pre-stabilized Co nanoparticles were deposited on SiO_x substrates from suspensions in toluene.[35] STM indicated that a closed layer of the particles was obtained. Figure 6 displays the MIES (a) and UPS (b) spectra of the surface-deposited, pre-stabilized Co nanoparticles as a function of surface temperature. Also shown are the energetic positions of the main structures resulting from step (1). For completeness, we have also indicated where the spectral features from carbonate (CO_3) groups bound to metallic surfaces[36] should be seen.

Below 250 °C some emission must still be attributed to the ionization of π-type MOs from the aromatic rings of residual toluene solvent molecules on the surface of the particles. From the comparison of the results at higher temperatures with those for gas-exposed planar Co films we estimate that most of the intensity observed in the valence band region (about 70%) is due to (Co–CO_x), with the rest being due to (Co–O) bonds.

For the formation of networks from Pt colloids the existence of an intact Al-organic colloidal protection shell is vital. The reactive methylaluminum groups present in the protecting shell provide the possibility to substitute organic groups at the Al; for the interlinking of the nanoparticles via organic spacer molecules these substituents must be bifunctional. The heating of Al-organic stabilized Pt nanoparticles with in situ control of MIES and UPS (HeI) has provided important information on the thermal properties of the Al-organic stabilization.[37] When heating a colloid network film consisting of Pt nanoparticles cross-linked by hydroquinone spacers, MIES shows the disappearance of the π-emission from the aromatic rings of the spacer molecules at binding energies, E_b, of between 4 and 8 eV. XPS, on the other hand, only indicates a small, unspecific change in the C 1s and O 1s intensities. This suggests the destruction of the spacer molecules (above 200 °C). Moreover, intensity develops at the Fermi level in the MIES spectra. This indicates that the Pt colloids (featuring metallic properties) become accessible to the He* probe atoms utilized for MIES. For temperatures above 200 °C the MIES spectra between E_b = 5 and 10 eV start to resemble more and more those of Al_2O_3 films.[36] This suggests that, as a consequence of the heating procedure, the Pt colloids are surrounded by some sort of (Al–O) network. This implies that most of the emission seen between E_b = 5 and 10 eV after heating would then be due to the ionization of O 2p orbitals from oxygen atoms of the (Al–O) network surrounding the Pt nanoparticles. XPS provides evidence that the Pt nanoparticles are present on the Si substrate employed for deposition up to 600 °C, although they are now stabilized by a Al–O network which has no bifunctional character anymore.

Spacer Molecules

Characterization of the Nanoparticle–Spacer Interaction by MIES and UPS

Some applications require a shell of organic molecules, in particular when the sintering of nanoparticles has to be avoided. Moreover, nanoparticle–organic spacer complexes are natural building blocks for networks of nanoparticles. Both applications impose similar problems for their characterization: the functional group, responsible for the nanoparticle–OM (OM: organic molecule) bond has to be iden-

tified, and the thermal stability of this bond has to be studied. Essentially the same procedure as described above for the pre-stabilization of the nanoparticles can be pursued, namely a comparison must be made with the fingerprint spectra obtained from the interaction of the same OMs (or at least originating from OMs with the same functional groups) with a planar surface possessing the same termination (the same "shell", see above) as the employed nanoparticles.

Here, we concentrate on the nanoparticle–spacer complexes as the peptization of nanoparticles by long-chain carboxylic acids (possessing a carbonyl group as functional unit) has been dealt with elsewhere.[35]

For illustration, Figure 7 presents MIES and UPS (HeI) spectra for Pt colloids cross-linked by hydroquinone (left) and chlorohydroquinone (right) spacers. For the as-prepared films there is practically no emission for binding energies smaller than 3.5 eV. Together with the fact that the work function of the as-prepared films is 4 eV (as estimated from the low-energy onset of the MIES spectra), we conclude that the studied films possess insulating character, with a bandgap of 7.5 eV. We have not interpreted the MIES/UPS spectra for binding energies above 11.5 eV because this range of binding energies is strongly affected by contributions from secondary and backscattered electrons The coarse structure of the MIES spectra for both networks was identified by comparison with fingerprint spectra available for *p*-CPC films (CPC = *para*-comylphenyl cyanate) on silicon.[38,39] While the MIES/UPS spectra from *p*-CPC show rather well-resolved fine structure due to the ionization of the π-MOs of the aromatic rings in particular, the present spectra show at most indications of a fine structure. From this comparison, we conclude that the emission between 4 and 11 eV is largely due to the ionization of the π- and σ-MOs of the aromatic rings in the spacers. In particular, the emission between 4 and about 8 eV is largely due to the ionization of the π-MOs. Apparently, as the inspection of Figure 7 shows, the main effect of the chlorination of the spacer molecules is a reduction of the emission in the range between 4 and 8 eV, i.e. a reduction in the emission from the ionization of the π-MOs. In addition, we see some fine structure in the MIES spectra in the range E_b = 3 to 7 eV which, as the comparison with the MIES results for 4(2)-CBM (CBM = conduction band minimum) suggests,[40] must be attributed to the ionization of the Cl 3p orbitals.

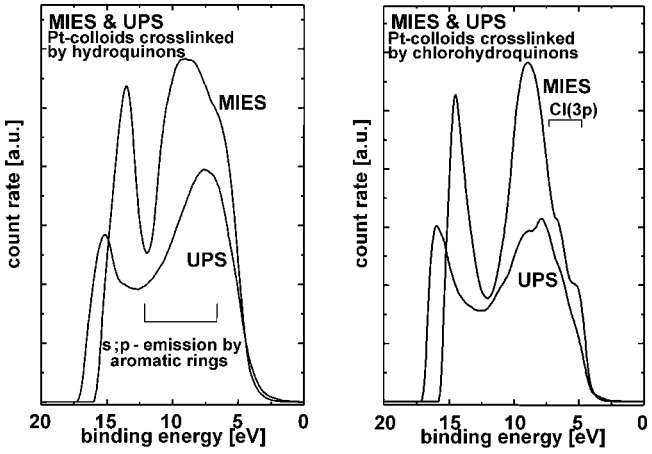

Figure 7. MIES and UPS (HeI) spectra for Al-organic-stabilized Pt colloids cross-linked with hydroquinone (left) and chlorohydroquinone (right) spacers.

Another instructive example for the study of the core–shell interaction is the functionalization of Pd nanoparticles by NR_4Cl molecules (R denotes alkyl groups of different length).[41] The reduction of metal salts with tetraalkylammonium hydrotriorganoborates is a general method for the preparation of metal colloids of elements of groups 6 to 11 in organic solvents. During the colloid formation, the stabilizing tetraalkylammonium salts are formed directly at the reduction center and act as powerful protecting agents for the metal particles. In early publications it was assumed that the protecting groups coordinate to the negatively charged metal cores of the colloid through NR_4 (model 1). The combination of X-ray absorption near edge structure (XANES) measurements with MIES and UPS (HeI) results suggests that the coordination of the stabilizing agent at the particle surface through metal–chlorine bonds is the more appropriate stabilization mode (model 2):[41] if model (1) were applicable, a comparatively well-localized spectral feature from the ionization of the Cl 3p atomic orbital should be seen in the MIES spectra at about E_B = 6 eV because the He* probe atom employed for MIES should interact with the charge cloud of the Cl atom.

Characterization of Pt Colloid Networks

TEM, ASAXS, BET, Modeling

The cross-linked Pt particles form solids which have been investigated by TEM. Comparison of TEM images of the cross-linked samples with those of simply protected Pt colloids show that the particle size of the colloids as well as their monodispersity have not changed after cross-linking (see Figure 8). Furthermore, particles seem to have larger distances between each other if larger spacer molecules are used.

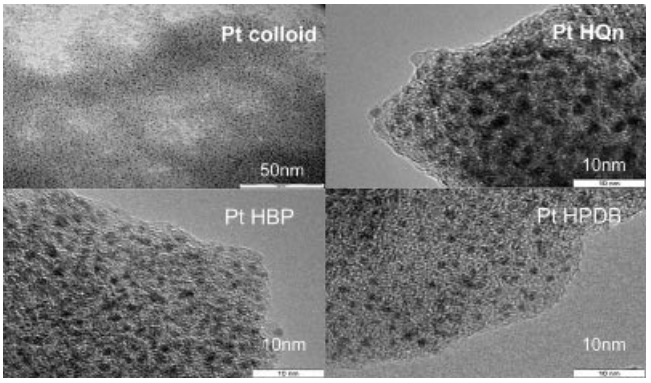

Figure 8. TEM images of protected Pt colloid particles and Pt particles cross-linked with HQn, HBP, and HPDB.

 © 2005 Wiley-VCH Verlag GmbH & Co. KGaA, Weinheim

Because of the large side-chains of Pt/HBDB and Pt/HPDP, one might expect a more linear rather than a three-dimensional network. The TEM images of these samples indeed show areas where one could assume such a chain-like linear arrangement of the particles. The particles are lined up in one direction with more or less identical distances (see part d of Figure 8).

Nitrogen sorption analyses have been used to investigate whether accessible pore systems are obtained after the cross-linking of the Pt particles. The results show that a mesopore system is formed for Pt/HBP (50 °C) with an average pore size of about 31 nm and a pore volume of 0.4680 $cm^3 g^{-1}$. For Pt/HBP2 (25 °C), the pore volume is only 0.0696 $cm^3 g^{-1}$ with an average pore size of only 18 nm. These results show that the temperature applied during the network formation has an influence on the density of the pore system formed. For the networks with the larger molecules HBDP and HPDP, the amount of nitrogen adsorbed in physisorption experiments is extremely low, indicating that no accessible pore system has formed. This can be explained by the large -$OC_{12}H_{25}$ side-chains of the spacer molecules which probably block the pore entrances and the space between the colloid particles.

The small-angle X-ray scattering curves of different cross-linked samples at different energies (ASAXS) are shown in Figure 9.

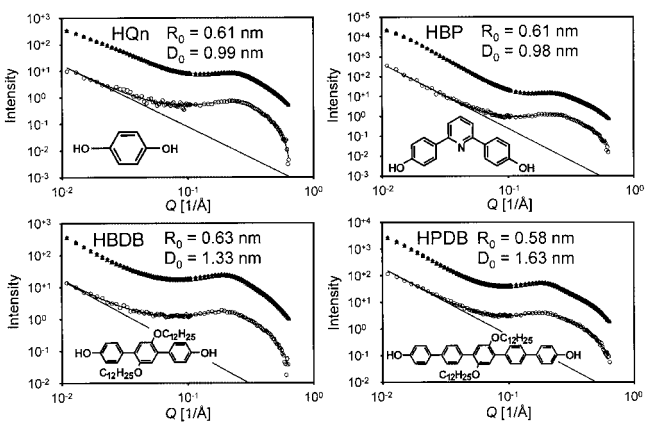

Figure 9. ASAXS curves of Pt particles cross-linked with different spacer molecules. For each plot, the lower curve (circles) is always the difference between the two upper curves (triangles) measured at two different energies (11437 and 11535 eV).

For the modeling of the scattering curves, a modified version of the so-called local monodisperse approximation (Pedersen[42]) is used:

$$\frac{d\sigma}{d\Omega}(Q) = \Delta\rho^2 \int_0^\infty N(D)\left(\int_0^\infty \Phi^2(Q,R) S(Q,R,D,t_{PS}) N(R)\,dR\right) dD$$

where $\Delta\rho^2$ is the scattering contrast, and t_{PS} (= 0.18 nm) is the thickness of the Al-organic protecting shell, which was determined in an earlier study.[16] $\Phi^2(Q,R)$ is the particle form-factor for a sphere of radius R, where

$$\Phi(Q,R) = 3\frac{\sin(QR) - QR\cos(QR)}{(QR)^3} V_0(R),$$

and $V_0(R)$ is the particle volume. $N(R)$ is the log-normal size distribution of the platinum particles

$$N(R) = \frac{1}{\sqrt{2\pi}\sigma R} \exp\left[-\frac{1}{2\sigma^2}\ln^2\left(\frac{R}{R_0}\right)\right],$$

where σ is the half-width at half maximum (HWHM) parameter of the size distribution, and R_0 is the most frequently occurring radius. $N(D)$ is the distribution of the surface-to-surface distances D, which has to be taken into account due to the high flexibility of the spacer molecules. Here, $N(D)$ is modeled by the Gaussian distribution

$$N(D) = \frac{1}{\sqrt{2\pi}\sigma_g} \exp\left[-\frac{1}{2\sigma_g^2}(D - D_0)^2\right],$$

where D_0 denotes the mean distance (spacer–molecule length) between two particles and σ_g is the HWHM of the Gaussian distribution. The structure factor $S(Q, R, D, t_{PS})$ is given by

$$S(Q,R,D,t_{PS}) = (1 + 24\eta G(QL)/(QL))^{-1},$$

(see, for example, Kinning and Thomas[43]), where L is the distance between two particles of radius R,

$$L = 2R + 2t_{PS} + D,$$

η is the volume fraction of a sphere of radius $L/2$, and

$$\begin{aligned} G(A) = {} & \alpha(\sin(A) - A\cos(A))/A^2 \\ & + \beta(2A\sin(A) + (2 - A^2)\cos(A) - 2)/A^3 \\ & + \gamma(-A^4\cos(A) + 4[(3A^2 - 6)\cos(A) + (A^3 - 6A)\sin(A) + 6])/A^5 \end{aligned}$$

with

$$\alpha = (1 + 2\eta)^2/(1 - \eta)^4$$
$$\beta = -6\eta(1 + \eta/2)^2/(1 - \eta)^2$$
$$\gamma = \eta\alpha/2.$$

The scattering behavior at low Q-values is modeled by a Q^{-p} power law, where p is the Porod exponent. This power law provides information on the whole particle system in the sample. The refined structure parameters for the seven samples are given in Table 2.

The Pt particle radii, R_0, as well as the polydispersities, σ, of all samples are in excellent agreement with one another. This can be expected, since the Pt particles used for the preparation of the nanoparticle networks stem from the same synthesis. The scattering contrast parameters, $\Delta\rho^2$, reflect, in general, the different volume fractions of the nanoparticle networks, and show therefore the same trend as the η parameters. The surface-to-surface distances, D_0, show partly significant differences between samples where the same spacer molecule was used for the interconnection of the Pt particles (HPDB, HPDB-2, and HBDB, HBDB-2).

 © 2005 Wiley-VCH Verlag GmbH & Co. KGaA, Weinheim

Table 2. Refined structure parameters for a Pt colloid cross-linked with different spacer molecules according to the Pedersen model.

Sample	R_0 [nm]	σ	D_0 [nm]	σ_g [nm]	$\Delta\rho$ [10^{-4} nm^{-2}]	η	P
HQn	0.50(9)	0.021(8)	0.59(3)	0.10(1)	2.02(2)	0.142(7)	2.07(13)
HBP	0.50(9)	0.021(12)	0.64(3)	0.01(1)	1.82(3)	0.135(12)	3.18(11)
HBP-2	0.51(9)	0.021(9)	0.70(2)	0.01(1)	1.93(2)	0.139(8)	3.22(8)
HBDB	0.52(9)	0.020(8)	0.70(6)	0.01(1)	1.17(3)	0.108(9)	1.90(12)
HBDB-2	0.53(6)	0.019(5)	1.00(5)	0.07(4)	1.39(1)	0.118(6)	2.04(11)
HPDB	0.54(4)	0.020(3)	1.29(9)	0.37(9)	2.05(2)	0.143(7)	2.37(5)
HPDB-2	0.54(5)	0.021(4)	0.96(6)	0.30(1)	1.28(1)	0.113(5)	2.43(16)

The HWHM parameters, σ_g, are also quite different, so that the distance distributions range from almost delta-shaped functions (σ_g = 0.01 nm) to quite broad distributions (σ_g = 0.37 nm). These findings may indicate that these flexible and rather complex spacer molecules are extremely sensitive to small differences in the sample preparation process. The Porod exponents, p, show that the nanoparticle networks of most samples form chain-like structures ($p \approx 2$), and only for the samples HBP and HBP-2 is an exponent of $p \approx 3$ obtained, which indicates the formation of more compact structures (e.g., surface fractals). In order to crosscheck the conclusions drawn from the Porod exponents, the pair-correlation functions $g(r)$ were calculated from the structure factors according to

$$g(r) = 1 + \frac{1}{2\pi^2 c_0}\int_0^\infty (S(Q,R,t_{PS},D)-1)\frac{\sin(Qr)}{Qr}Q^2 dQ\,.$$

The Pt particle concentration, c_0, is readily obtained from the relation

$$c_0 = \frac{\eta}{V_{HS}}$$

where the hard-sphere volume, V_{HS}, is given by

$$V_{HS} = \frac{\pi}{6}\int_0^\infty N(D)\left(\int_0^\infty N(R)L^3 dR\right)dD$$

$$= \frac{\pi}{6}\int_0^\infty N(D)\left(\int_0^\infty N(R)[2R + 2t_{PS} + D]^3 dR\right)dD\,.$$

Formal coordination numbers $\langle Z\rangle$ are obtained by integration of $g(r)$ over the volume of the first coordination shell:

$$\langle Z\rangle = 4\pi c_0 \int_{r_0-\Delta}^{r_0+\Delta} g(r) r^2 dr$$

where $g(r_0) = max$, and 2Δ is the total width of the coordination peak. Although the coordination numbers will probably not be correct on an absolute scale due to the influence of the polydispersities of the particles and the spacer molecules on the shape of the coordination peak, a qualitative comparison between the different samples is still possible.[16]

The particle concentrations, c_0, hard-sphere volumes, coordination-peak positions, r_0, and the average coordination numbers $\langle Z\rangle$ are given in Table 3.

Table 3. Particle concentrations, c_0, hard-sphere volumes, coordination-peak positions, r_0, and the average coordination numbers, $\langle Z\rangle$, of Pt particles cross-linked with different spacer molecules.

Sample	c_0 [10^{-2} nm^{-3}]	V_{HS} [10^1 nm^3]	r_0 [nm]	$\langle Z\rangle$
HQn	3.38(68)	0.42(8)	2.4(5)	2.4(4)
HBP	3.00(60)	0.45(9)	2.5(5)	2.1(4)
HBP-2	2.83(56)	0.49(9)	2.5(5)	2.2(4)
HBDB	2.10(42)	0.51(10)	2.6(5)	1.6(3)
HBDB-2	1.51(30)	0.79(15)	2.9(6)	1.6(3)
HPDB	1.24(25)	1.16(23)	3.3(6)	2.2(5)
HPDB-2	1.43(28)	0.79(15)	3.0(6)	1.8(4)

The lowest values for the coordination numbers are obtained for those samples with lowest Porod exponents, and higher coordination numbers correspond to larger Porod exponents, i.e. to the networks forming more compact structures. Thus, the results confirm that the scattering contributions at low Q-values are sufficiently well described by the power laws and that the above conclusions are obviously correct.

A further crosscheck of the least-squares results can be obtained from the Fourier transform of the SAXS intensities, the so-called radial distance distribution function[44]

$$\gamma(r) = \frac{r^2}{J_0}\int_0^\infty \frac{d\sigma}{d\Omega}(Q)\frac{\sin(Qr)}{Qr}Q^2 dQ\,,$$

where J_0 is the total scattering power

$$J_0 = \int_0^\infty \frac{d\sigma}{d\Omega}(Q)Q^2 dQ\,.$$

This function contains information on the particle sizes, and interparticle distances. Here, the particle radii are simply given by the corresponding maxima of the first peaks at $\gamma(r = R_1)$. Together with the maxima of the second peaks (at $r = R_2$), the interparticle distances ($d = R_2 - R_1$) and the surface-to-surface distances ($D_0 = d - 2R_1 - 2t_{PS}$) are readily obtained.[16] These values are of course only crude approximations, since the determination of particle radii and/or interparticle distances from the radial distance distribution functions is only reasonable for the case of monodisperse particle systems. Table 4 summarizes the results from the analysis of the distance distribution functions. The parameters are found to be consistent with those obtained from the least-squares analysis, and the significant differences in the D_0 compared to the least-squares results can be attributed to the influence of the particle-size and

 © 2005 Wiley-VCH Verlag GmbH & Co. KGaA, Weinheim

spacer-length distributions, as well as the moderate data quality (the average relative e.s.d.'s for the SAXS intensities are around 15%), which is also reflected by the fairly large e.s.d's of the refined least-squares model parameters (see Table 4).

Table 4. Structure parameters of Pt particles cross-linked with different spacer molecules calculated by the Fourier transform method.

Sample	J_0 [cm^{-1} nm^{-3}]	R_1 [nm]	R_2 [nm]	d [nm]	D_0 [nm]
HQn	20(1)	0.6(1)	3.0(1)	2.4(2)	0.8(3)
HBP	15(1)	0.6(1)	3.0(1)	2.4(2)	0.8(3)
HBP-2	53(1)	0.6(1)	3.1(1)	2.5(2)	0.9(3)
HBDB	45(1)	0.6(1)	3.4(1)	2.8(2)	1.2(3)
HBDB-2	65(1)	0.6(1)	4.0(1)	3.4(2)	1.8(3)
HPDB	135(27)	0.6(1)	4.0(1)	3.4(2)	1.8(3)
HPDB-2	52(1)	0.7(1)	4.1(1)	3.4(2)	1.6(3)

Modeling of the Pt–Spacer Interaction

The interparticle distances analyzed by ASAXS were compared to those calculated from constructed Pt network structures. The spacer lengths were calculated using the MNDO method.[45] The construction of the network structures is based on the assumption of the presence of an Al-organic monolayer on the particle surface, while the corresponding bond lengths were taken from the literature and the Cambridge Structural Database: (1) Al–Pt: 0.232 nm;[46] (2) Al–C: 0.187 nm; (3) Al–O: 0.232 nm. The thus-constructed Pt nanoparticles (1.2 nm) with the cross-linked spacers BDM and HPDB are illustrated in Figures 10 and 11, respectively.

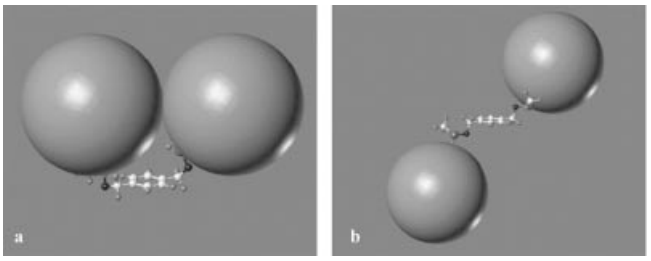

Figure 10. Modeled Pt–spacer–Pt units with BDM as the spacer: a) the minimum interparticle distance; b) the maximum interparticle distance.

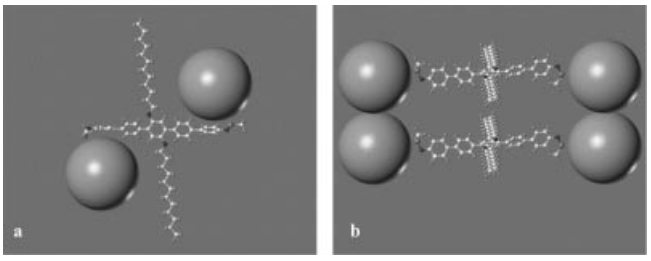

Figure 11. Modeled Pt–spacer–Pt units with HPDB as the spacer: a) the minimum interparticle distance; b) the maximum interparticle distance (another extreme case of minimum particle distance between different interlaced subunits is also shown).

Considering the rotation of Al–O bonds, two extremes are possible, namely the minimum and maximum interparticle distance, although another extreme case of minimum interparticle distance between different interlaced subunits is also shown in Figure 11b. Thus, one has to keep in mind that interparticle distances do not necessarily correspond to the length of the molecular spacers in the obtained network. The more flexible the spacer molecules and the anchoring group, the broader the particle–particle distance distribution is expected to be.

XAFS Characterization of Networked Particles

X-ray absorption spectroscopy can contribute in two ways to the characterization of networked particles, either indirectly, as the (partial) decomposition of the surfactant shell in a networked system should lead to notably reduced rates of agglomeration, and directly, if changes in the electronic structure and the geometry of the metal particles are observed. The indirect characterization is discussed in detail in ref.,[47] therefore here only the main results obtained from XAFS are summarized briefly considering Figures 12 and 13.

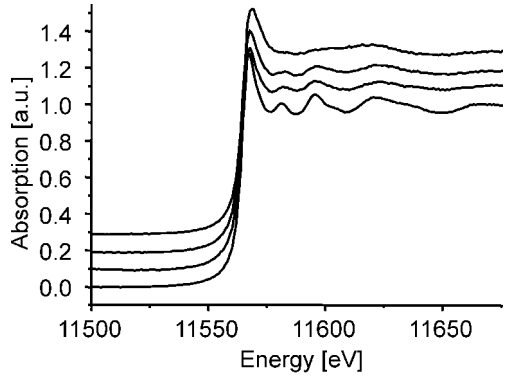

Figure 12. Pt colloid before cross-linking at (from top to bottom) room temperature, 160 °C, and 300 °C in comparison with a Pt foil reference (bottom).

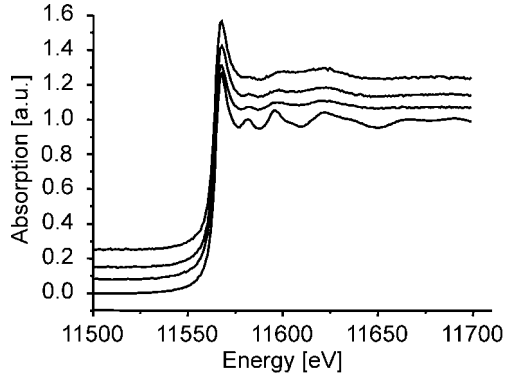

Figure 13. Pt colloid, cross-linked with chlorophenol at (from top to bottom) room temperature, 160 °C, and 300 °C in comparison with a Pt foil reference (bottom).

As the actual intensity of the shape resonances typical for platinum metal allows a rough qualitative estimate of the particle size and degree of ordering present in the sam-

 © 2005 Wiley-VCH Verlag GmbH & Co. KGaA, Weinheim

ple, size-effects and effects of varying spacer molecules at different temperatures can be separated from each other. Only for the unmodified colloid does one observe a significant increase in the intensity of the shape resonances starting at 160 °C, which indicates that the particles undergo significant agglomeration processes at this temperature. In contrast to that, the system with a chlorophenol spacer shows a much smaller trend towards agglomeration even at 300 °C.

At the same time, it is worth noting that the room temperature spectra displayed in Figures 12 and 13 show differences in the white-line region, especially the maximum intensity of the white line and the shape of its high energy slope. The different white-line features change as a function of time in different ways: whereas the agglomerating particles feature a more and more intense white line upon approaching a status more similar to the bulk, the reverse is observed in the cross-linked system. This proves that the observed temperature-dependent changes in the electronic structure shown in Figures 12 and 13 are predominantly due to changes in the decomposing surfactant shell of the colloidal particles, whereas the spacers effectively prevent agglomeration.

With respect to the direct characterization, at first sight it may seem surprising that any changes in the structure of the particles occur at all as a consequence of the networking process even though such changes are clearly visible, as evident from the example presented in Figure 4, where the white-line intensity is increased notably and appears slightly shifted to lower energy, whereas the shape resonance region of the spectra is hardly influenced by the network formation with this type of spacer molecule. TEM studies verify that, in contrast to the situation encountered after the system has been exposed to thermal stress, which was discussed in the above paragraph, the geometry parameters of the individual cores, such as size and shape, remain identical. In addition, the connection of individual metal cores by spacer molecules leads to a preferred interparticular distance although not (necessarily) to a highly ordered long range structure, in which modification of electronic structure can be envisioned due to the necessity to introduce periodic boundary conditions.

Nevertheless, on looking at the Pt L_3-edge XANES spectra displayed in Figure 4 it is evident that the effects of spacer-induced changes in the electronic structure are observed. Therefore, the only explanation for such changes is that the surfactant shell around the particle core is restructured, either geometrically or with respect to the charge distribution, in such a way that considerable influence is exerted on the metal atoms. It is important to stress the implications of this statement, because it means that information on the particle size and shape [as obtained typically from TEM, but also using (A)SAXS] and the nature of the core [as obtained frequently using a diffraction-based technique, such as XRD (X-ray diffraction) or SAED (selected area electron diffraction)] is not sufficient to describe the nature of a nanoparticle, which in turn explains why the macroscopic (e.g. magnetic) properties determined by different researchers on particles of equal size and phase can vary drastically. In fact, a number of theoretical predictions and experimental results based on various experimental techniques,[48–51] including X-ray absorption spectroscopy,[52–57] can be found in the literature to describe such effects. Specifically, a more detailed review on such effects in general is found in ref.,[28] the width of accessible modifications. for example for the case of Co nanoparticles, is discussed in ref.,[56] and a detailed model how these changes influence electronic structure in terms of magnetic properties of Co particles is presented in ref.[57]

Returning to the class of particles discussed in this work, clearly such a modification must be traceable even more directly in the aluminum organic shell. In fact, as shown for selected examples in Figure 14, and discussed in more detail in ref.,[33] the cross-linking with sebacic acid leads to a dramatic change in the electronic structure of Al, increasing the intensity of the white-line drastically and shifting its energy position to a value typical for sixfold (oxygen) coordinated Al. At the same time, the changes induced by cross-linking with a mixture of decanol and sebacic acid spacers lead to a similar trend in the spectra, but to a notably smaller extent. All of these experimental results underline that a spacer-dependent, controlled change in the protection shell is in fact observed, which is especially pronounced when sebacylic acid is used, which leads to a didentate coordination of the spacer to the Al and a sixfold oxygen coordination, but less significant when the connection between the aluminum organic shell and spacer molecule involves just the OH bond.

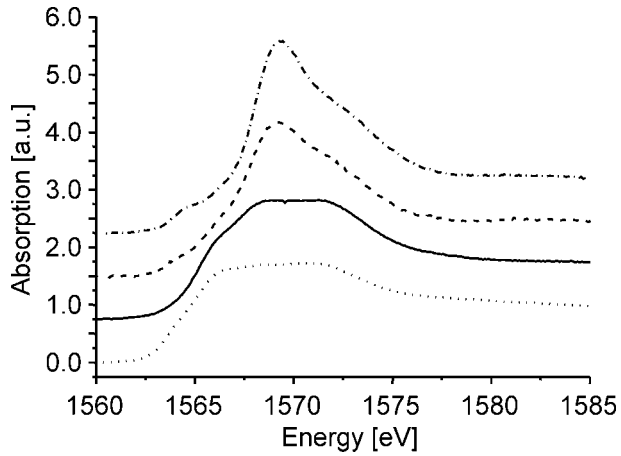

Figure 14. Al K XANES spectra of (from top to bottom) a Pt colloid networked with sebacic acid, the same networked with a mixture of decanol and sebacic acid, the same before networking, and trioctylaluminum.

As discussed in ref.,[33] an almost identical behavior is observed for a related system based on Co nanoparticle precursors, emphasizing once again that one is dealing with a spacer-induced effect on the aluminum organic shell that is dependent on the exact nature of the spacer molecule.

In fact, these differences are also reflected in the Pt L_3 EXAFS evaluation of particles after cross-linking with sebacic acid and HBP, respectively, as shown in Figure 5.

 © 2005 Wiley-VCH Verlag GmbH & Co. KGaA, Weinheim

Table 1 compares the results of this analysis for two such particles, one cross-linked with sebacic acid and the other with HBP. In contrast to the situation encountered for sebacic acid, where it is necessary to use an additional soft backscatterer like oxygen in the fit, this is not the case for HBP. At the same time, the presence of the HBP spacer seems to influence the Pt–Pt distance, which differs beyond the uncertainty of the fitting result and is increased almost to bulk level. As the core of the particles is only 1.2 nm in diameter, such a change can easily be attributed to a variation in core–surfactant interaction as a function of the local charge density on the aluminum atom. Consequently, a controlled tuning of the structure of the Pt core appears possible by choosing the spacer molecules. In fact, the multiplicity of choices becomes evident when looking at the variety of spectral signatures in the white-line region as a function of the spacer molecule, as shown in Figure 15. In combination with a detailed understanding of such effects, this may open a novel approach towards catalysts that are optimized in terms of both activity and accessibility of the catalytic centers.

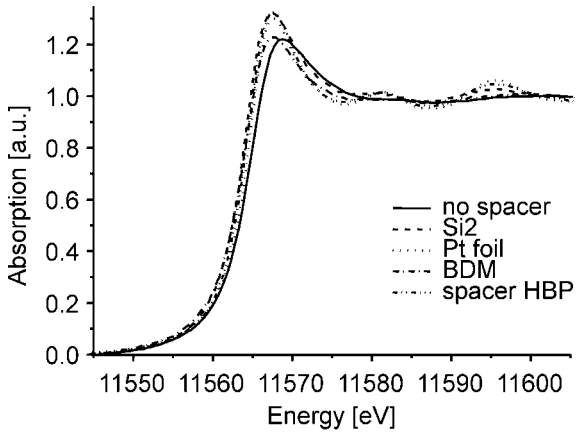

Figure 15. Pt L_3 XANES spectra of colloids with varying spacer molecules and a foil reference.

MIES and UPS Investigations

The obvious problems faced during the characterization of nanoparticle networks produced by a "bottom-up" strategy are threefold:

· Verification of the presence of the spacer molecules in the assembled network;

· Given the presence of the spacers in the nanoparticle–spacer compound, the bonding between the nanoparticles and the spacers needs to be verified;

· The verification of an ordered network composed of nanoparticles and spacers.

As far as the first point is concerned, the main task to be done is to distinguish between the spectral contributions from the organic molecules (OMs) of the particle's shell (Al-organic stabilization in the present case) and those from the spacers. A simple approach is the use of appropriately labeled spacers, i.e. those having a particular ligand atom attached to that produces a clear spectral signature that is well-separated from any of those from the OMs present in the shell. This strategy is similar to that illustrated above for the study of the interaction between and Pt and Pd nanoparticles with their respective protection shells (see above).

The verification of a link between a spacer and adjacent nanoparticles follows the strategy outlined above for obtaining information on the bond formation between nanoparticles and species forming their shell or between nanoparticles and spacer molecules. As a necessary condition, it can be stated that no free, unreacted functional groups (intended for bond formation with the nanoparticles) should be detectable by MIES. However, it is advisable to obtain topological information on the existence of an ordered nanoparticle–spacer structure in addition to the electronic structure information. Our strategy consists in combining MIES/UPS with STM and STS.

STM Investigations

For illustration, we present results for Pt nanoparticles interlinked by HBDB spacers. Figure 16 shows the STM results for Pt nanoparticles (about 1 nm average diameter, as determined by TEM) interlinked by the spacer molecules. The average size of the detected, close-packed aggregates is typically 7 nm. However, the ordered array seen in Figure 16 is apparently not that of single Pt nanoparticles separated by spacers, therefore each aggregate must consist of several interlinked Pt nanoparticles. The simplest structural unit producing aggregates of 7 nm consists of six Pt nanoparticles clustered around a central Pt nanoparticle. Interestingly, we find such compact structures very seldom. This indicates that the nanoparticle networks consist mainly of 1D structures, such as chains, that would escape detection by STM. This agrees with the ASAXS results, which indeed indicate that the nanoparticle networks of most samples consist of chain-like structures (see above).

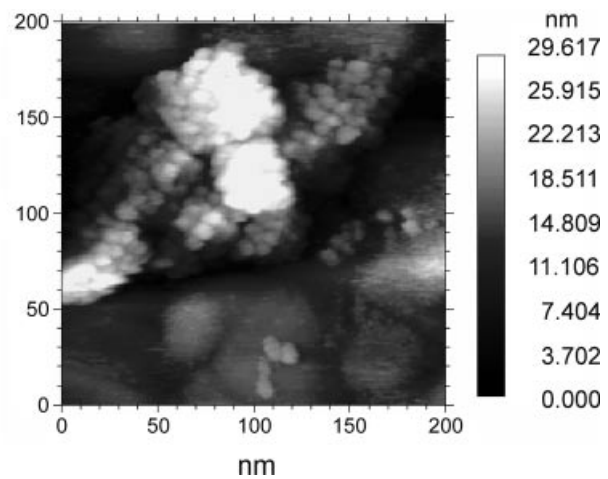

Figure 16. STM image of Pt nanoparticles (average diameter 1 nm) interlinked by HBDB spacers deposited on an Au substrate.

STS measurements, performed as a function of the temperature of the substrate onto which the nanoparticle array is deposited, confirm that the network structure possesses insulating behavior up to 200 °C. More detailed infor-

 © 2005 Wiley-VCH Verlag GmbH & Co. KGaA, Weinheim

mation on the electronic structure of the network is furnished by the MIES/UPS spectra. They confirm the insulating character of the structure, which possesses a bandgap width of about 7 eV and gives spectra (not shown) similar to those of Figure 7.

Summary

Combining different analytical methods, such as TEM, ASAXS, UPS, MIES, XAFS, Sorption analysis, and STM, has allowed us to gain insights into the processes taking place during the network formation of nanoparticles cross-linked with different spacer molecules. Several new spacers with different molecular lengths and rigidity have been used to cross-link Pt colloids via protonolytic reaction to prepare network materials. In general, the materials that form upon cross-linking show no long-range order but rather form network-like structures. When using rigid molecular spacers such as those described above, TEM investigations have revealed that short-length spacers give rise to a densely packed material while long and rigid molecular spacers tend to produce 1D-type structures where the interparticle distance is considerably larger. These results are corroborated by ASAXS investigations. Physical sorption analyses have shown that mesoporous materials are produced for some systems. The shapes of the hysteresis loops of the sorption isotherms strongly depend on the type of molecular spacer used and also on the preparative conditions. Isotherms recorded on products prepared from long-length molecular spacers show that these materials hardly adsorb nitrogen. This is due to the blocking effect from the organic species and poorly defined porous structures. ASAXS measurements have revealed that the interparticle distance only reflects the conformation of the molecular spacers. Varying the preparative conditions with each defined molecular spacer leads to diverse pore structures but identical interparticle distances.

Significant differences between the electronic structures of Pt nanoparticles pre-stabilized with an Al-organic shell and cross-linked particles are observed at room temperature. The properties of the metallic nanoparticles are thus directly influenced by changes of the protective shell. Furthermore, it has proved possible to analyze subtle changes in the protecting shell. Although the Pt colloid modified with 3-chlorohydroquinone differs only in the additional cluster located on the second end of the space molecule, the chlorine can only be detected by MIES in the latter case, thus indicating different equilibrium positions of this molecule. Thermal treatment leads to a disintegration of the spacer molecules, as could be shown by MIES and XANES spectroscopy. A clear trend towards the formation of shape resonances under thermal loads is observed only for the unmodified particles. This indicates that it is driven not by agglomeration but by mere structural reordering within the colloidal metal cores. This agglomeration does not occur as easily for particles that are initially surrounded by spacer molecules, even after destruction of the spacer molecules. It was possible to correlate this observation to a suggested formation of an Al–O protecting shell by MIES.

Acknowledgments

The authors would like to thank Dr. Görigk from the JUSIFA Beamline at the Hasylab, Hamburg, for technical support. Furthermore, we would like to thank Mr. Spliethoff, Mr. Dreier, and Dr. Tesche from the MPI für Kohlenforschung for providing the electron micrographs and Dr. Weidenthaler from the MPI für Kohlenforschung for XPS and XRD investigations. Financial support of the Deutsche Forschungsgemeinschaft, Priority Program SPP 1072 (grant nos. Bo 1135, Ho 887, and Ke 155), and of the Max-Planck-Gesellschaft is gratefully acknowledged.

[1] M. T. Reetz, M. Winter, B. Tesche, *Chem. Commun.* **1997**, 147.
[2] T. Sato, D. Brown, B. F. G. Johnson, *Chem. Commun.* **1997**, 1007.
[3] G. Schmidt, M. Bäumle, N. Beyer, *Angew. Chem. Int. Ed.* **2000**, *39*, 182.
[4] G. Schön, U. Simon, *Colloid Polym. Sci.* **1995**, *273*, 101.
[5] G. Schön, U. Simon, *Colloid Polym. Sci.* **1995**, *273*, 202.
[6] A. Taleb, C. Petit, M. P. Pileni, *Chem. Mater.* **1997**, *9*, 950.
[7] L. Motte, F. Billoudet, E. Lacaze, J. Doulin, M. P. Pileni, *J. Phys. Chem. B* **1997**, *101*, 138.
[8] X. M. Lin, C. M. Sorensen, K. J. Klabunde, *Chem. Mater.* **1999**, *11*, 198.
[9] M. Brust, D. Bethell, D. J. Schiffrin, C. J. Kiely, *Adv. Mater.* **1995**, *7*, 795.
[10] W. Shenton, S. A. Davis, S. Mann, *Adv. Mater.* **1999**, *11*, 449.
[11] S. Connolly, D. Fitzmaurice, *Adv. Mater.* **1999**, *11*, 1202.
[12] B. A. Korgel, S. Fulham, S. Connolly, D. Fitzmaurice, *J. Phys. Chem. B* **1998**, *102*, 8379.
[13] H. Bönnemann, W. Brijoux, R. Brinkmann, U. Endruschat, W. Hofstadt, K. Angermund, *Rev. Roum. Chim.* **1999**, *44*, 1003.
[14] H. Bönnemann, W. Brijoux, R. Brinkmann, German Patent WO 99/59713 (**1999**).
[15] H. Bönnemann, N. Waldöfner, H.-G. Haubold, T. Vad, *Chem. Mater.* **2002**, *14*, 1115.
[16] T. Vad, H.-G. Haubold, N. Waldöfner, H. Bönnemann, *J. Appl. Crystallogr.* **2002**, *35*, 459.
[17] N. Gourdoupi, A. K. Andreopoulou, V. Deimede, J. K. Kallitsis, *Chem. Mater.* **2003**, *15*, 5044.
[18] F. Kakali, J. Kallitsis, T. Pakula, G. Wegner, *Macromolecules* **1998**, *31*, 6190.
[19] H.-G. Haubold, K. Gruenhagen, M. Wagener, H. Jungbluth, H. Heer, A. Pfeil, H. Rongen, G. Brandenberg, R. Moeller, J. Matzerath, P. Hiller, H. Halling, *Rev. Sci. Instr.* **1989**, *60*, 1943.
[20] H. Modrow, S. Bucher, J. Hormes, R. Brinkmann, H. Bönnemann, *J. Phys. Chem. B* **2003**, *107*, 3684.
[21] C. S. S. R. Kumar, M. Aghasyan, H. Modrow, E. Doomes, C. Henke, J. Hormes, R. C. Tittsworth, *J. Nanopart. Res.* **2004**, *6*, 369.
[22] E. A. Stern, M. Newville, B. Ravel, Y. Yacoby, D. Haskel, *Physica B* **1995**, *209*, 117; M. Newville, P. Livins, Y. Yacoby, J. J. Rehr, E. A. Stern, *Phys. Rev. B* **1993**, *47*, 14126; M. Newville, B. Ravel, D. Haskel, E. A. Stern, Y. Yacoby, *Physica B* **1995**, *209*, 145.
[23] Y. Harada, S. Masuda, H. Ozaki, *Chem. Rev.* **1997**, *97*, 1897.
[24] H. Morgner, *Adv. At. Mol. Opt. Phy.* **2000**, *42*, 387.
[25] S. Dieckhoff, V. Schlett, W. Possart, O.-D. Hennemann, J. Günster, V. Kempter, *Appl. Surf. Sci.* **1996**, *103*, 221.
[26] D. Ochs, M. Brause, W. Maus-Friedrichs, V. Kempter, V. Puchin, A. Shluger, L. Kantorovich, *Surf. Sci.* **1996**, *365*, 557.
[27] L. Kantorovich, A. L. Shluger, P. V. Sushko, J. Günster, P. Stracke, D. W. Goodman, V. Kempter, *Faraday Discuss.* **1999**, *114*, 173.

 © 2005 Wiley-VCH Verlag GmbH & Co. KGaA, Weinheim

[28] H. Modrow, *Appl. Spectrosc. Rev.* **2004**, *39*, 183.
[29] A. Di Cicco, M. Berrettoni, S. Stiza, E. Bonetti, G. Cocco, *Phys. Rev. B* **1995**, *50*, 12386.
[30] Y. A. Babanov, L. V. Golovschikova, F. Boscherini, T. Haubold, S. Mobilio, *Nucl. Instrum. Methods. Phys. Res. A* **1995**, *359*, 321.
[31] P. Fornasini, S. A. Beccara, G. Dalba, R. Grisenti, A. Sanson, M. Vaccari, F. Rocca, *Phys. Rev. B* **2004**, *70*, 174301.
[32] K. Angermund, M. Bühl, U. Endruschat, F. T. Mauschick, R. Mörtel, R. Mynott, B. Tesche, N. Waldöfner, H. Bönnemann, G. Köhl, H. Modrow, J. Hormes, E. Dinjus, F. Gassner, H.-G. Haubold, T. Vad, *J. Phys. Chem. B* **2003**, *107*, 7507.
[33] H. Modrow, S. Modrow, J. Hormes, N. Waldöfner, H. Bönnemann, *J. Phys. Chem. B* **2005**, *109*, 900.
[34] M. Frerichs, F. X. Schweiger, M. Maus-Friedrichs, V. Kempter, *Surf. Interface Anal.*, submitted.
[35] S. Rudenkiy, M. Frerichs, F. Voigts, W. Maus-Friedrichs, V. Kempter, R. Brinkmann, N. Matoussevitch, W. Brijoux, H. Bönnemann, N. Palina, H. Modrow, *Appl. Organomet. Chem.* **2004**, *18*, 553.
[36] D. Ochs, M. Brause, W. Maus-Friedrichs, V. Kempter, *J. Electron Spectrosc. Relat. Phenom.* **1998**, *88–91*, 725.
[37] L. Beuermann, W. Maus-Friedrichs, S. Krischok, V. Kempter, S. Bucher, H. Modrow, J. Hormes, N. Waldöfner, H. Bönnemann, *Appl. Organomet. Chem.* **2003**, *17*, 268.
[38] S. Dieckhoff, V. Schlett, W. Possart, O.-D. Hennemann, J. Günster, V. Kempter, *Appl. Surf. Sci.* **1996**, *103*, 221.
[39] S. Dieckhoff, R. Höper, V. Schlett, T. Gesang, W. Possart, O.-D. Hennemann, J. Günster, V. Kempter, *Fresenius J. Anal. Chem.* **1997**, *358*, 258.
[40] J. Stultz, S. Krischok, D. W. Goodman, *Langmuir* **2002**, *18*, 2962.
[41] S. Bucher, J. Hormes, H. Modrow, R. Brinkmann, N. Waldöfner, H. Bönnemann, L. Beuermann, S. Krischok, W. Maus-Friedrichs, V. Kempter, *Surf. Sci.* **2001**, *497*, 321.
[42] J. S. Pedersen, *J. Appl. Crystallogr.* **1994**, *27*, 595.
[43] D. J. Kinning, E. L. Thomas, *Macromolecules* **1984**, *17*, 1712.
[44] L. A. Feigin, D. I. Svergun, *Structure Analysis by Small Angle X-ray and Neutron Scattering*, Plenum Press, New York, **1987**, 38–40.
[45] H. G. Haubold, X. H. Wang, G. Goerigk, W. Schilling, *J. Appl. Crystallogr.* **1997**, *30*, 653.
[46] D. Bakowies, W. Thiel, *J. Comput. Chem.* **1996**, *17*, 87.
[47] L. Beuermann, W. Maus-Friedrichs, S. Krischok, V. Kempter, S. Bucher, H. Modrow, J. Hormes, N. Waldöfner, H. Bönnemann, *Appl. Organomet. Chem.* **2003**, *17*, 268.
[48] C. R. Vestal, Z. J. Zhang, *J. Am. Chem. Soc.* **2003**, *125*, 63.
[49] V. Torma, O. Vidoni, U. Simon, G. Schmid, *Eur. J. Inorg. Chem.* **2003**, 1121.
[50] S. Link, A. Furube, M. B. Mohamed, T. Asahi, H. Masuhara, M. A. El Sayed, *J. Phys. Chem. B* **2002**, *106*, 945.
[51] Y. Diamant, S. G. Chen, O. Melamed, A. Zaban, *J. Phys. Chem. B* **2003**, *107*, 1977.
[52] A. L. Ankudinov, J. J. Rehr, J. Low, S. Bare, *Phys. Rev. Lett.* **2001**, *86*, 1642.
[53] T. Rajh, L. X. Chen, O. Melamed, A. Zaban, *J. Phys. Chem. B* **2002**, *106*, 10543.
[54] P. Zhang, T. K. Sham, *Phys. Rev. Lett.* **2003**, *90*, 245502.
[55] S. Bucher, J. Hormes, H. Modrow, R. Brinkmann, N. Waldöfner, H. Bönnemann, L. Beuermann, S. Krischok, W. Maus-Friedrichs, V. Kempter, *Surf. Sci.* **2002**, *497*, 321.
[56] O. Margeat, C. Amiens, B. Chaudret, P. Lecante, R. E. Benfield, *Chem. Mater.* **2005**, *17*, 107.
[57] J. Hormes, H. Modrow, H. Bönnemann, C. S. S. R. Kumar, *J. Appl. Phys.* in print (**2005**).

Received: May 17, 2005
Published Online: August 24, 2005

 © 2005 Wiley-VCH Verlag GmbH & Co. KGaA, Weinheim